

LARGE APERTURE O I 6300 Å OBSERVATIONS OF COMET HYAKUTAKE: IMPLICATIONS FOR THE PHOTOCHEMISTRY OF OH AND O I PRODUCTION IN COMET HALE-BOPP

JEFFREY P. MORGENTHALER,¹ WALTER M. HARRIS,¹ AND MICHAEL R. COMBI²

Received 2006 September 22; accepted 2006 November 20

ABSTRACT

In previous work (Morgenthaler et al. and Glinski et al.), we proposed a revision to the standard OH photochemistry of van Dishoeck & Dalgarno in order to explain the anomalously bright [O I] 6300 Å emission observed by several instruments in comet C/1995 O1 (Hale-Bopp). In order to test the validity of revisions to the OH photochemistry, we present wide-field Fabry-Pérot [O I] 6300 Å observations of comet C/1996 B2 (Hyakutake) and review similar observations recorded for 1P/Halley and 1989 c1 (Austin). Conventional long-slit spectroscopic observations of several comets in [O I] are also reviewed. The bulk of the evidence suggests that the OH photochemical rates of van Dishoeck & Dalgarno are, on the whole, correct and that the bright [O I] emission observed in Hale-Bopp, particularly at cometocentric distances beyond $\sim 3 \times 10^4$ km, was unique to that comet, or possibly any comet with such a large production rate.

Subject headings: comets: individual (Hale-Bopp, Hyakutake, Austin, Halley) — instrumentation: spectrographs — molecular data — molecular processes

1. INTRODUCTION

By virtue of its greater production rate than other outgassing species inside 2.5 AU of the Sun, water is considered the principal constituent of comets. Water is observable with ground-based remote sensing techniques (e.g., Dello Russo et al. 2004), however, the sensitivity and field of view (FOV) of these techniques is limited. Therefore, the photochemical daughters of H₂O, O, OH, and H, are typically used as proxies. Water production rates, $Q(\text{H}_2\text{O})$, as well as coma dynamic parameters, such as outflow velocities, are derived using measurements of O, OH, and H, and, where available, H₂O itself. Both H and OH have solar photon-induced resonances from their ground states that are detectable from ground-based observatories: H α at 6562 Å (e.g., Smyth et al. 1993), the 0–0 band of the $A^2\Sigma^+ - X^2\Pi$ transition of OH at 3080 Å (e.g., Schleicher & Osip 2002), and the Λ -doublet transitions of OH at 18 cm (e.g., Crovisier et al. 2002). Accessible to space-based observatories are the resonant transitions Ly α at 1216 Å (e.g., Combi et al. 2000) and O I 1304 Å (e.g., McPhate et al. 1999; Brittacher et al. 2001) and the OH 1–0 band at 2800 Å (e.g., Weaver et al. 1981). Atomic oxygen lacks resonant lines that are accessible from ground-based observatories but does have three metastable lines: the singlet 5577 Å ($^1S \rightarrow ^1D$) and the doublet $\lambda\lambda$ 6300/6364 Å ($^1D \rightarrow ^3P$). At the densities of a cometary coma, the most likely mechanism for oxygen to enter the metastable state is by photodissociation of a molecule such as H₂O, OH, or CO₂ (Festou & Feldman 1981). With metastable lifetimes of < 1 s for O(1S) and ~ 110 s for O(1D) (Froese Fischer & Saha 1983), over most of a cometary coma, the transitions out of the metastable state can be considered prompt. The preferred decay path of O(1S) is through O(1D), and 6300 Å is the brighter of the $^1D \rightarrow ^3P$ doublet lines by a factor of 3.0 ± 0.1 (Cochran & Cochran 2001; Capria et al. 2005). In our studies, which have concentrated on the use of the metastable oxygen line [O I] 6300 Å (hereafter [O I]) as a proxy for $Q(\text{H}_2\text{O})$ (Huppler et al. 1975; Scherb 1981; Magee-Sauer et al. 1990; Schultz et al. 1992; Morgenthaler et al. 2001).

The particle densities in cometary comas are sufficiently low that O(1D) is not collisionally excited (although it can be quenched; e.g., Streit et al. 1976). For this reason, [O I] emission is a direct tracer of the site of a single photochemical reaction. Unlike resonant fluorescent emissions, photodissociation rates are not subject to significant Swings and Greenstein effects. This makes the conversion of [O I] data into $Q(\text{H}_2\text{O})$ values simple. From the average [O I] surface brightness, I_{6300} , over a particular FOV, Ω , and a geocentric distance, Δ , we derive total production rate of O(1D) photons, $Q[\text{O}(\mathit{^1D})]$,

$$Q[\text{O}(\mathit{^1D})] = (4/3)(4\pi\Delta^2\Omega I_{6300})AC, \quad (1)$$

where the factor of 4/3 corrects for the emission in the 6364 Å line, and AC is the aperture correction for emission outside the FOV. Using only photodissociation branching ratios of H₂O to O(1D), H₂O to OH, and OH to O(1D) (BR n ; see Table 1) and equation (1), [O I] aperture photometry can be easily converted into a H₂O production rate:

$$Q(\text{H}_2\text{O}) = \frac{Q[\text{O}(\mathit{^1D})]}{\text{BR1} + (\text{BR2})(\text{BR3})}, \quad (2)$$

assuming H₂O is the dominant source of [O I] in comets. Assuming a photochemical source of [O I], [O I] image data shows where the photodestruction of oxygen-bearing species is occurring.

It was within the context of these simple assumptions that Morgenthaler et al. (2001) interpreted [O I] observations of comet C/1995 O1 (Hale-Bopp). Using Fabry-Pérot (FP) spectroscopic data from the newly commissioned Wisconsin H α Mapper (WHAM) telescope and equations (1) and (2), Morgenthaler et al. derived $Q(\text{H}_2\text{O})$ values a factor of 3–4 higher than those published by other groups (open triangles in Fig. 6 of Morgenthaler et al. 2001). The combination of Hale-Bopp’s large surface brightness, geocentric distance, and the sensitive WHAM 1° diameter FOV allowed WHAM to capture essentially all of the [O I] emission from comet Hale-Bopp (i.e., AC = 1). The WHAM observations were confirmed by independent FP observations at the McMath-Pierce solar telescope facility and multiobject spectroscopy

¹ Department of Earth and Space Sciences, University of Washington, Seattle, WA.

² Department of Atmospheric, Oceanic, and Space Sciences, University of Michigan, Ann Arbor, MI.

TABLE 1
PHOTODISSOCIATION BRANCHING RATIOS

Reaction	BR n	Quiet Sun	Active Sun	Ref.
$\text{H}_2\text{O} + h\nu \rightarrow \text{H}_2 + \text{O}(^1D)$	BR1	0.050	0.067	H
$\text{H}_2\text{O} + h\nu \rightarrow \text{H} + \text{OH}$	BR2	0.855	0.801	H
$\text{OH} + h\nu \rightarrow \text{H} + \text{O}(^1D)$	BR3	0.094	0.176	H
$\text{OH} + h\nu \rightarrow \text{H} + \text{O}(^1D)$	BR3 _G	0.192	...	G
$\text{OH} + h\nu \rightarrow \text{H} + \text{O}(^1D)$	BR3 _M	0.357	...	M
$\text{OH} + h\nu \rightarrow \text{H} + \text{O}(^3P)$	BR4	0.662	0.513	H
$\text{OH} + h\nu \rightarrow \text{H} + \text{O}(^3P)$	BR4 _G	0.785	...	G
$\text{OH} + h\nu \rightarrow \text{H} + \text{O}(^3P)$	BR4 _M	0.472	...	M

REFERENCES.—(H) Huebner et al. 1992; (M) Morgenthaler et al. 2001; (G) Glinski et al. (2004).

from the WIYN³ telescope (Figs. 6 and 7 of Morgenthaler et al. 2001). Assuming the Hale-Bopp $Q(\text{H}_2\text{O})$ values derived by other groups to be correct, Morgenthaler et al. proposed one or both of the following possibilities to explain the discrepancy: (1) there is a source of [O I] in the outer coma that is unknown or has been previously ignored, or (2) there is an error in the standard model of OH photochemistry previously undetected by narrower FOV measurements. The main photochemical sources for additional [O I] considered by Morgenthaler et al. included contributions from CO_2 and CO. These did not yield $Q[\text{O}(^1D)]$ values that would rival those of H_2O and OH by a factor of 3–4. A distributed source of H_2O in the form of large particles ejected isotropically from the Hale-Bopp nucleus was also considered. In addition to the objections to this hypothesis raised by Morgenthaler et al., we note that the eventual decay of such particles to hydrogen would be detected by the *Solar and Heliospheric Observatory (SOHO)* SWAN Ly α all-sky monitor and would have been included in the $Q(\text{H}_2\text{O})$ values derived by Combi et al. (2000) and the wide-field OH measurements of Harris et al. (2002). Finding no obvious source for the excess [O I] emission, Morgenthaler et al. turned to the laboratory OH cross section-measurements of Nee & Lee (1984) as evidence to support possibility (2), the modification of OH photochemistry. A boost in BR3 to the value BR3_M, (listed in Table 1) solved the problem, at least for Hale-Bopp. Subsequent work by Glinski et al. (2004) found that the inner coma of Hale-Bopp was dense enough to support an unexpectedly high O_2 production rate by collisions between ground-state oxygen and OH. O_2 photodissociation is very efficient at producing [O I]. The calculations of Glinski et al. were able to match the Hale-Bopp [O I] profile reasonably well and required a smaller boost in the value of BR3 (BR3_G in Table 1). The revisions to BR3 and BR4 proposed by Glinski et al. and Morgenthaler et al. also imply modification to the total OH photochemical lifetime (listed in Table 2).

In this work we present previously unpublished [O I] observations of comet C/1996 B2 (Hyakutake) and a reanalysis of [O I] observations of comet 1P/Halley and 1989 c1 (Austin) to test the validity of revisions to the van Dishoeck & Dalgarno (1984) OH photochemistry.

2. OBSERVATION AND DATA REDUCTION

Observations of comet C/1996 B2 (Hyakutake) were made by the WHAM telescope in 1996 March and April during its com-

³ The WIYN Observatory is a joint facility of the University of Wisconsin–Madison, Indiana University, Yale University, and the National Optical Astronomy Observatories.

TABLE 2
QUIET-SUN OH PHOTODISSOCIATION CALCULATIONS

Reference ^a	BR3 ^b	BR4 ^c	$\tau_{\text{OH}}^{\text{d}}$ (ks)
van Dishoeck & Dalgarno (1984).....	0.048	0.718	120
H/VD (BR3).....	0.094	0.662	134
M (BR3 _M).....	0.357	0.472	85
G (BR3 _G).....	0.192	0.785	91

^a VD: using van Dishoeck & Dalgarno (1984) theoretical OH cross sections; H/VD: treatment of VD cross sections by Huebner et al. (1992); M: Morgenthaler et al. (2001) values; G: Glinski et al. (2004) values.

^b $\text{OH} + h\nu \rightarrow \text{H} + \text{O}(^1D)$.

^c $\text{OH} + h\nu \rightarrow \text{H} + \text{O}(^3P)$.

^d OH lifetime.

missioning phase at Pine Bluff Observatory in Pine Bluff, Wisconsin. WHAM is a wide-field (1° diameter FOV) dual-etalon FP system that can be operated as a spectrometer with a resolving power $\lambda/\Delta\lambda \sim 3 \times 10^4$ (10 km s^{-1}) and free spectral range of $\sim 3 \text{ \AA}$ in the red (6300–6500 Å) or as a tunable narrowband imager with an adjustable passband. WHAM can detect a field-filling emission line source in the red of as little as 0.1 R in a 30 s exposure. WHAM’s primary design goal has been to map the warm ionized medium in the Galaxy, using $\text{H}\alpha$ emission as a proxy (Reynolds 1997, 2002; Haffner et al. 2003). Its combination of features also make it ideal for cometary coma studies.

2.1. Spectroscopy

Spectroscopic observations of NGC 7000 at $\text{H}\alpha$ form the basis of the WHAM sensitivity calibration. A transfer calibration factor of 0.986 is used to move from $\text{H}\alpha$ to [O I] 6300 Å (Scherb 1981; Reynolds et al. 1998; Morgenthaler et al. 2001). For the Hyakutake campaign, $\text{H}\alpha$ observations were recorded 1996 March 21–23. The March 21 and 22 data, together with the WHAM sensitivity derived from several years worth of NGC 7000 observations, suggest an extinction coefficient of 0.152 mag airmass⁻¹ in the red. One spectrum of Hyakutake in [O I] was recorded March 23 (Fig. 1, left) and 12 on April 9 (Fig. 1, right, one shown). The spectra were fitted with Voigt profiles to determine the effective surface brightness in the WHAM FOV. The two March 23 NGC 7000 observations were unexpectedly 20% high (not accountable with any reasonable extinction coefficient). A similar “blip” was observed in two of the Hyakutake [O I] spectra observed on April 9 (but not in their airglow profiles). We attribute this behavior to instrumental problems in the commissioning phase and assign a 20% systematic uncertainty to our surface brightness results. One of the April 9 spectra gave particularly low surface brightness values (including the airglow). Sky conditions were noted as variable in the observing logs, so we attribute this to passing clouds. The remaining April 9 spectra, recorded over a period of ~ 45 minutes and a change in airmass of ~ 1 , were individually airmass corrected and fitted to obtain airglow and cometary [O I] surface brightness values. The fitted values were averaged and their standard deviation was used as a measure of the uncertainty. The observing parameters and surface brightness values are shown in the first eight rows of Table 3. The 10 s exposure times on April 9 imply a sensitivity of $\sim 1 R$, which is consistent with the standard deviation in the data. All data were recorded with the comet centered in the 1° WHAM FOV to a precision of $\sim 1'$. The size of the FOV and short exposure times (30 s for March 23 and 10 s for April 9) alleviated the need for active tracking or guiding, even with Hyakutake’s fast apparent motion.

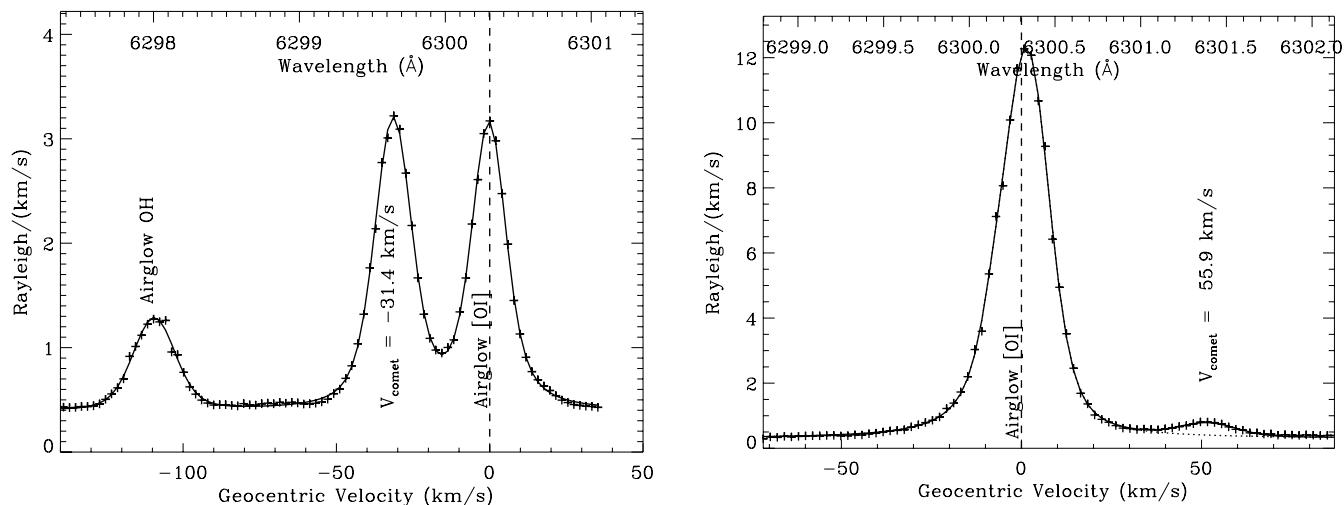


FIG. 1.—WHAM spectra of comet Hyakutake on 1996 March 23 (*left*) and 1996 April 9 (*right*). Voigt profiles are fitted to the data (*solid line*), with the continuum underlying the April 9 data shown as a dotted line.

The WHAM calibration in spectroscopic mode assumes a spatially flat, field-filling source, such as Galactic H α emission. Because the WHAM spectrometer is, in fact, more sensitive to emission near the center of its FOV, an increment to the sensitivity, IS, must be applied for objects with centrally peaked emission. IS can be derived by multiplying a normalized image of the object by the normalized sensitivity map of the WHAM spectrometer (Fig. 2 of Morgenthaler et al. 2001). The quality of the Hyakutake images was not sufficient to apply this technique directly. Rather, radial profiles of the images served as guides for model fits (see § 3), which were then transformed into synthetic comet images. Since a broad family of models fit the data reasonably well, we assign systematic uncertainty of at most 10% to our values of IS.

TABLE 3
COMET HYAKUTAKE [O I] OBSERVATIONS AND RESULTS

Parameters	1996 March 23 Values	1996 April 9 Values
UT.....	07:30	03:00
Air mass.....	1.08	2.75
Heliocentric R (km).....	1.084	0.711
Geocentric Δ (km).....	0.121	0.498
\dot{R} (km s $^{-1}$).....	-35.9	-41.1
$\dot{\Delta}$ (km s $^{-1}$).....	-31.4	55.9
Airglow (R).....	50	270
Raw comet I_{6300} (R).....	50.3 ± 1.0	8.2 ± 1.1
IS ^a	1.4	1.5
Comet I_{6300} (R).....	36 ± 0.7	5.4 ± 0.7
Projected FOV radius (km).....	157,000	654,000
$Q_{\text{obs}}[\text{O}(^1D)]$ (mol s $^{-1}$) ^b	3.8×10^{28}	1.0×10^{29}
$Q_{\text{mod}}[\text{O}(^1D)]$ (mol s $^{-1}$) ^{b,c}	4.8×10^{28}	7.0×10^{28}
Aperture correction (AC) ^c	1.52	1.01
$Q(\text{H}_2\text{O})$ using BR3 (mol s $^{-1}$).....	4.4×10^{29}	1.3×10^{30}
$Q(\text{H}_2\text{O})$ using BR3 _G (mol s $^{-1}$).....	2.7×10^{29}	4.7×10^{29}
$Q(\text{H}_2\text{O})$ using BR3 _M (mol s $^{-1}$).....	1.6×10^{29}	2.9×10^{29}
$Q(\text{H}_2\text{O})$ (Combi et al. 2005).....	4.6×10^{29}	1.2×10^{30}
$Q(\text{H}_2\text{O})$ (Schleicher & Osip 2002).....	1.9×10^{29}	1.8×10^{29d}
$Q(\text{H}_2\text{O})$ (Hicks & Fink 1997).....	3.1×10^{29}	4.7×10^{29e}

^a Increment to instrument sensitivity due to centrally peaked source.

^b In observed FOV.

^c Calculated using BR3 and Combi et al. (2005) variation in $Q(\text{H}_2\text{O})$.

^d From 1996 April 14.

^e From 1996 April 11.

2.2. Images

WHAM image-mode observations of comet Hyakutake were recorded 1996 March 21, 23, and April 9. The design of WHAM calls for an adjustable iris, which limits the bandpass of light transmitted in image mode. During the commissioning phase, this iris was only available on March 23. Proper observing protocol requires on- and off-line images to be taken on and off the comet. A variety of circumstances prevented these protocols from being completed, although on March 23 only the off-line off-comet image is missing. For a tunable FP, such as WHAM, on- and off-line images can be recorded without changing the narrowband order separating filter, so in principle, one image, recorded using a bright atmospheric line such as the airglow [O I], provides a reasonable flat-field image for reduction of all the on- and off-line images. However, our experience with detailed calibration in support of the WHAM Hale-Bopp observations (Morgenthaler et al. 2001) showed that there are subtle shape differences with different iris settings and tunes. For the Hyakutake data, the best available flat-field image was an off-line sky image recorded on 1996 April 9, which had a spectral coverage of ~ 150 km s $^{-1}$. The airglow line fell at the red end of this spectrum.

The March 23 image-mode data were recorded with a 14 mm iris installed in the instrument that limited the bandwidth to ~ 30 km s $^{-1}$. This allowed clean isolation of the cometary [O I] line from the cometary NH $_2$ and airglow OH lines. The airglow [O I], however, was still an important contributor. On-line comet and sky images and an off-line comet image was recorded, but no off-line sky image was recorded. The image of the sky recorded in the on-line sky image is clearly brighter than sky recorded in the on-line comet image. We attribute this to a change in sky conditions and/or a slight change in the instrument tune toward the red. Using the edges of the images as a guide, we find a scaling factor of 0.5 brings the sky image to a reasonable value. Using the same procedure, a factor of 0.06 was applied to this image to emulate an off-line sky image, which was subtracted from the off-line comet image. Because of the bandwidth-limiting iris, the off-line comet image of March 23, sky subtracted in this way, contains a clean measure of the continuum emission contributing to the sky-subtracted [O I] image. We found the centers of the images using a two-dimensional Gaussian fit program, with final subpixels “tweaks” applied by looking at the quadrant-by-quadrant radial profiles. The sky-subtracted off-line image was translated to overlap with sky-subtracted on-line image. The resulting

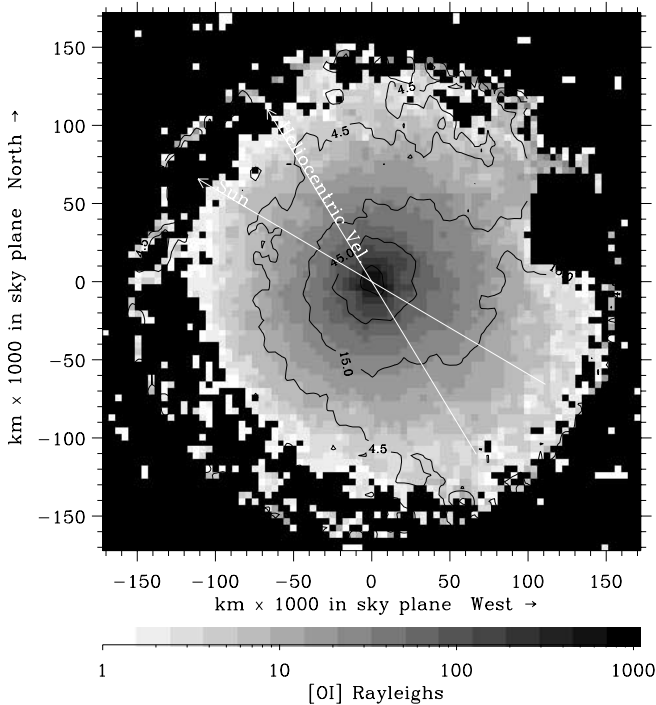


FIG. 2.—WHAM images of comet Hyakutake in [O I] and continuum recorded on 1996 March 23. The gray scale shows the [O I] emission, and the contours show the dust. A star seen in both images at the right side of the image was masked out during processing.

continuum-subtracted [O I] image is shown in gray scale in Figure 2. The contours show the continuum image. Calibration of the March 23 image-mode observations was accomplished by noting that the [O I] emission effectively filled the WHAM 0.5° radius FOV. The total [O I] surface brightness detected in image mode should therefore be equivalent to the IS-corrected value in spectroscopic mode (see § 3). Neglecting the small contribution to the total flux in image mode lost by masking out the star seen in the right side of the [O I] and dust images, we calculated a conversion factor from detector units to rayleighs for the [O I] image and applied the same factor to the dust image. Quadrant-by-quadrant radial profiles obtained from the [O I] image in Figure 2 are shown in Figure 3.

Because the bandwidth-limiting iris was only installed in the instrument on March 23, analysis of the image-mode data collected March 21 and April 9 is more difficult to interpret. Comet images are required for derivation of the factors IS and AC, applied to the spectroscopic data, so we present the April 9 image-mode data. Without a bandwidth-limiting iris, the tune of the instrument was adjusted to shift the comet emission in and out of the image bandpass. The off-line images were recorded with the airglow line at the far red end of the bandpass. As discussed above, the off-line sky image became the flat-field image used to reduce all the image data. This same tune was used to record the off-line comet image. Since the airglow was unusually bright that evening (Table 3), the comet continuum was nearly completely washed out. In addition, the cometary NH_2 lines are included in this passband. The April 9 on-line comet [O I] image was recorded with the airglow line mostly pushed off of the blue end of the passband. No on-line sky image was recorded, and this is a very different tune than the other observations, so construction of an on-line sky image has been difficult. The 650,000 km FOV radius of the WHAM observations on April 9 is sufficiently large for us to assume the observations in the on-line image should result in a flux below

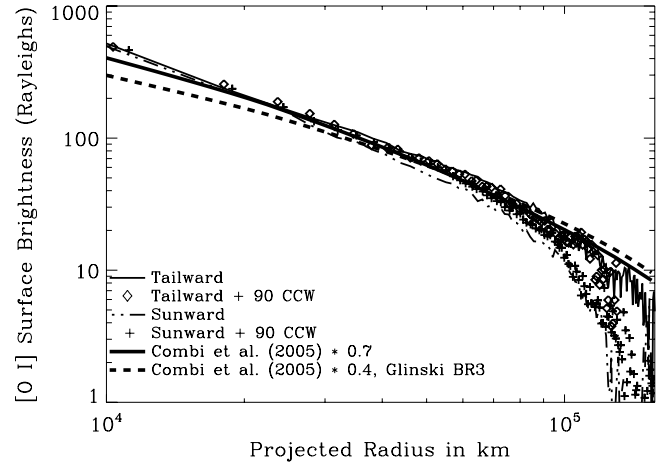


FIG. 3.—Quadrant-by-quadrant radial profile of Hyakutake [O I] emission on 1996 March 23. Two Haser models, discussed in the text, are overplotted. The model represented by the solid line was calculated using the standard van Dishoeck & Dalgarno (1984) value of BR3.

the image mode detection limit at the edge of the FOV. We therefore scale the off-line sky image and subtract it from the on-line comet image until a zero at the edges of the FOV is obtained. The best scaling factor is near 0.25. A similar technique is used to check the zero at the edge of the off-line comet image. In principle, the factor should be exactly 1, since the same passband is used. Using the same zero criterion, the best factor was 0.95, which is reasonable considering the time-varying nature of the [O I] airglow. The point-spread function (PSF) of the WHAM siderostat is of order a few WHAM $0.8'$ pixels and not steady

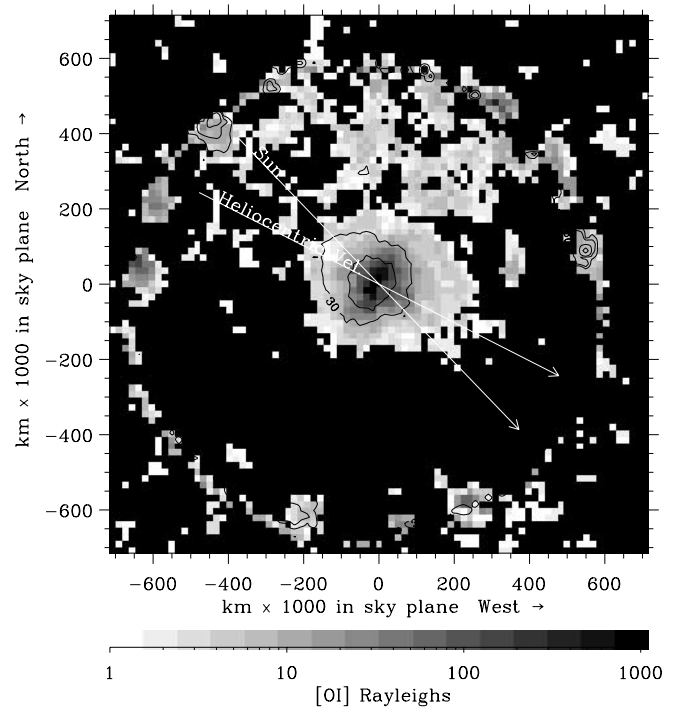


FIG. 4.—WHAM images of comet Hyakutake in continuum plus [O I] (gray scale) and continuum plus NH_2 (contours), recorded on 1996 April 9. The intensity scale for the [O I] plus continuum was derived from the [O I] spectroscopic data recorded on this night, assuming spectroscopic mode was sensitive to Hyakutake emission light only out to 200,000 km. The edge of the WHAM 1° diameter FOV is seen in the spurious contours toward the edge of the image. The gray-scale image appears compressed in the sunward direction because of distortion in the WHAM PSF for this look direction.

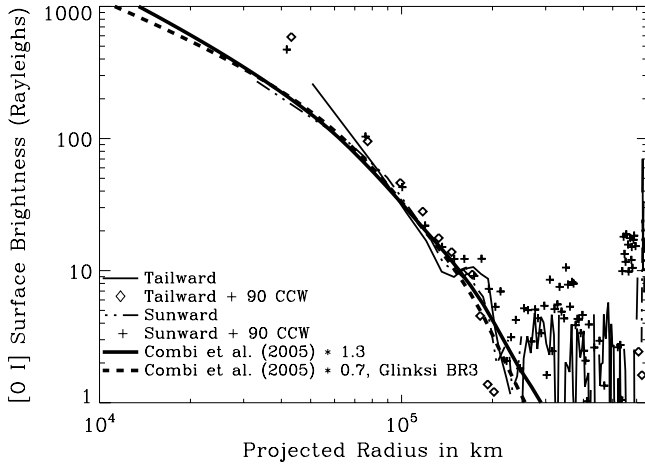


FIG. 5.—Quadrant-by-quadrant radial profile of [O I] plus continuum on 1996 April 9. Two Haser models, discussed in the text, are overplotted. The model represented by the solid line was calculated using the standard van Dishoeck & Dalgarno (1984) value of BR3. Data outside of 2×10^5 km indicate the extent of the positive excursions in the noise of the data. The points inside 8×10^4 km are likely to be effected by the highly nonuniform WHAM PSF in this look direction.

with look direction, so the central peak of the comet is not always round. This was a particularly pronounced effect for the April 9 comet observations. A two-dimensional Gaussian was fitted to the on-line and off-line images and the off-line image was translated with subpixel accuracy to line up with the on-line image. The resulting on-line and off-line images are shown in Figure 4, with their calibration determined as with the March 23 data. We attempted to subtract the off-line image from the on-line, but presumably because of the NH_2 emission and/or strong sky component, the on- and off-line images are of comparable intensity near the peak. The off-line image needed to be scaled down by a factor of 4 to obtain sensible results over any substantial scale length. We therefore did not subtract the off-line image and worked directly with the profile of the [O I] plus continuum image (Fig. 5) to help interpret the spectroscopic data.

The WHAM FOV is 0.5° in radius, or 650,000 km projected on the sky plane for Hyakutake on April 9. However, the image data in Figure 4 and its radial profile (Fig. 5) show that the instrument was sensitive to emission out to only 200,000 km. Application of equation (1) naturally compensates for the case when the FOV is larger than the emitting region because of the inverse proportionality between Ω and the surface brightness, I , of the enclosed source. However, when attempting to calibrate the image-mode data, it is critical to match the FOVs over which the effective surface brightness is calculated. We did this by multiplying the IS-corrected spectroscopic surface brightness (see § 3) by the factor of ~ 10 difference in assumed FOVs and arrived at an average image-mode flux for the [O I] plus continuum image per rayleigh in the [O I] line. We applied this same factor to convert the continuum plus NH_2 image to rayleighs as well.

3. ANALYSIS

Hyakutake was observed to have a very bursty water production rate, with $Q(\text{H}_2\text{O})$ values varying over factors of several on timescales as short as a day (e.g., Schleicher & Osip 2002; Combi et al. 2005). This complicates the comparison between data sets taken with varying FOV sizes and observation dates. Our primary solution to this problem is to calculate time-dependent [O I] Haser profiles generated with $Q(\text{H}_2\text{O})$ values taken from other work and compare them to radial profiles of our image data.

Our treatment of the one- and two-component time-dependent Haser model is similar to that of Magee-Sauer et al. (1988), except that in the two-component case, we adjust the bulk outflow velocity to match that of the daughter after 1 parent scale length. We use a numeric integrator to convert from particle number density as a function of cometocentric distance to column density as a function of projected cometocentric distance on the sky. This gives us the flexibility to easily include effects, such as quenching, that modify the basic Haser density profile, and experiment with the chemical reactions considered by Glinksi et al. (2004). We found that over the density ranges represented by our Hyakutake [O I] data, neither quenching nor chemical production of O_2 were significant.

We recognize that the Haser model does not have a firm basis in physical reality (e.g., compared to the vectorial model of Festou 1981); however, Combi et al. (2004) give formulas for the transformation between Haser and vectorial scale lengths, photochemical ejection velocities, and outflow velocities. Using these translations, good agreement between Haser, vectorial, and Monte Carlo model radial profiles is achieved. For all comets except Hale-Bopp, we adopt the H_2O outflow velocity, $v_{\text{H}_2\text{O}}$, of Budzien et al. (1994),

$$v_{\text{H}_2\text{O}} = 0.85R_h^{-1/2} \text{ km s}^{-1}, \quad (3)$$

where R_h is the heliocentric distance of the comet. We take the average ejection velocity of OH from the H_2O photodissociation event to be $v_e = 1.05 \text{ km s}^{-1}$ (Crovisier 1989). Using a H_2O lifetime for the quiet Sun at 1 AU of $82 \times 10^3 \text{ s}$ (Huebner et al. 1992), any of the OH lifetimes listed in Table 2, and the vectorial-to-Haser formulas of Combi et al. (2004), we derive an OH Haser outflow velocity of 1.3 km s^{-1} at 1 AU. Our Haser model code accepts time-varying R_h and $Q(\text{H}_2\text{O})$ and calculates the instantaneous outflow velocities and lifetimes of H_2O and OH as a function of cometocentric distance appropriate for a particular observation time. Photochemical lifetimes at 1 AU and branching ratios are input parameters to the code so that the thick solid and dotted lines in Figures 3 and 5 could be easily generated for the different cases we consider here. A final input parameter is a scaling factor that can be applied to the model to better match the data.

Model profiles parallel to the thick solid lines in Figures 3 and 5 were generated using the model described above, Combi et al. (2005) $Q(\text{H}_2\text{O})$ values, and standard OH photochemistry derived by Huebner et al. (1992) using the van Dishoeck & Dalgarno (1984) OH cross section. The heliocentric velocity changes by only a few kilometers per second between our observations, so we neglect the Swings effect. Scaling factors of 1.3 (March 23) and 0.7 (April 9) multiplying the model profiles were required in order to best match the data. These scaling factors are comparable to the systematic uncertainty in the spectroscopic data. There is likely to be an additional systematic uncertainty in the transfer calibration between image and spectroscopic mode, particularly on April 9. We attribute the difficulty of the model in fitting the data in the innermost points of both profiles to nonuniformities in the WHAM PSF. The April 9 profile is also likely contaminated by continuum and NH_2 emission, which have shorter scale lengths than [O I]. The outermost points in the March 23 data are likely contaminated by flat-fielding and sensitivity effects.

Using the model profiles discussed above, we generated synthetic comet images and multiplied by the WHAM sensitivity map (Morgenthaler et al. 2001, Fig. 2) to derive the increment to sensitivity values, IS (shown in Table 3). The values of AC were also derived using this model. Like IS, AC did not vary significantly

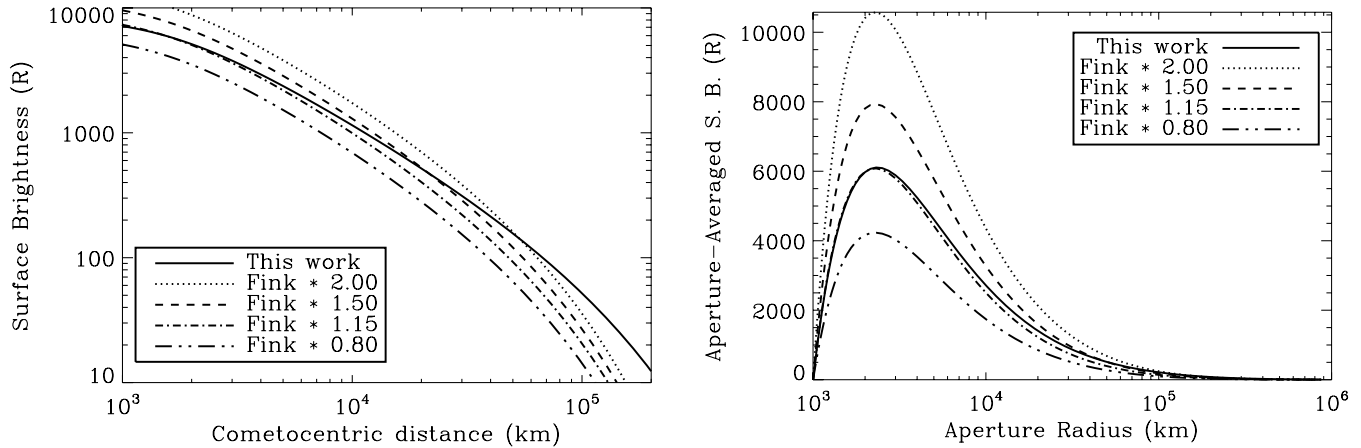


FIG. 6.— Comparison of the combined H_2O and OH Haser model used in this work to the H_2O -only model typically used by Fink and coworkers (e.g. Fink & Johnson 1984; Fink & Di Santi 1990; Fink & Hicks 1996) to fit measured [O I] profiles. Calculations are for a comet at 1 AU with $Q(\text{H}_2\text{O}) = 1 \times 10^{30} \text{ mol s}^{-1}$. Quenching of the [O I] transition is included, as can be seen by the roll-off of the profiles inside of 3000 km. The Fink model results have been multiplied by the values shown in the legend. The left panel shows that except inside of ~ 3000 km, the profiles diverge, due to the contribution of [O I] from OH and the slight difference in the assumed H_2O scale length. The right panel shows that an aperture summation applied to both profiles yields striking agreement for the case in which the Fink profile is multiplied by 1.15.

across the broad family of models that fit the radial profiles well. The dashed lines in Figures 3 and 5 were generated using BR3_G and the OH lifetime derived by Glinski et al. (2004; see also our Table 2). Particularly over the radial extent covered on March 23 data, the slope of the BR3_G -derived model is clearly flatter than the data. In order to achieve a good match to the data using BR3_G , the outflow velocity of H_2O at 1 AU would need to be 0.4 km s^{-1} , $v_{\text{OH}} = 1.1 \text{ km s}^{-1}$, and the model scaled by a factor of 0.3.

An alternate approach to our time-varying Haser models is to simply compare production rates derived by various methods on the same day. We must be cautious with this approach because of Hyakutake's highly variable production rate and the difference in effective aperture sizes of the measurements we compare. The *SOHO* SWAN instrument used by Combi et al. (2005) is an all-sky monitor. However, near-continuous temporal coverage in the observations and careful deconvolution techniques have allowed Combi et al. to infer the daily-averaged nuclear production rate of H_2O on nearly all the days of the Hyakutake perihelion passage. The OH observations of Schleicher & Osip (2002) and [O I] observations of Hicks & Fink (1997) were conducted over FOVs of less than $120''$. We treat the resulting $Q(\text{H}_2\text{O})$ values as instantaneous nuclear production rates. Schleicher & Osip have excellent time coverage, including observations on March 23 and April 14. Hicks & Fink also have several observations, including March 23 and April 11. To derive our $Q(\text{H}_2\text{O})$ values, we start with the observed $\text{O}(^1D)$ production rate over our entire FOV, $Q_{\text{obs}}[\text{O}(^1D)]$, which is derived using equation (1) and the values in Table 3 with $\text{AC} = 1$. For comparison, we calculate $Q_{\text{mod}}[\text{O}(^1D)]$, the $\text{O}(^1D)$ production rate in the FOV using our preferred model above (unscaled). Using equations (1) and (2) and the values in the table, including AC predicted from the preferred model above, we derive $Q(\text{H}_2\text{O})$ values for the OH branching ratios listed in Table 2. The last three lines in Table 3 show the $Q(\text{H}_2\text{O})$ values of Combi et al. (2005), Schleicher & Osip (2002), and Hicks & Fink (1997). We see that the standard OH photochemistry of van Dishoeck & Dalgarno (BR3) applied to the WHAM [O I] observations yields $Q(\text{H}_2\text{O})$ values consistent with those of Combi et al. The OH photochemistry modification proposed by Morgenthaler et al. (2001; BR3_M) yields results more similar to those of Schleicher & Osip. The Glinski et al. (2004) OH photochemistry modifications yield $Q(\text{H}_2\text{O})$ values closer to those of Hicks & Fink (1997).

4. DISCUSSION

The bursty nature of comet Hyakutake and disagreement between our $Q(\text{H}_2\text{O})$ calibration sources makes differentiation between proposed OH photochemistries difficult. We therefore turn to [O I] observations of other comets to test the effect that any modifications to BR3 and/or the total OH lifetime may have.

4.1. Long-Slit Observations

Since 1980, a group led by U. Fink at the Lunar and Planetary Laboratory of the University of Arizona has observed dozens of comets with conventional long-slit, moderate resolution spectroscopy (e.g., Fink & Johnson 1984; Fink & Hicks 1996). In general, the technique of long-slit spectroscopy is not well suited to cometary studies because of the mismatch between the shape of the object being studied and the entrance aperture of the instrument. In particular, for species such as [O I], which have extended radial profiles, order-of-magnitude corrections are necessary to convert from measured fluxes to production rates (e.g., Table 3 of Fink & Di Santi 1990). [O I] also presents a problem because of its proximity to cometary NH_2 lines and the bright [O I] air-glow. The motivation described in the work of Fink and collaborators (e.g., Fink & Johnson 1984; Fink & Di Santi 1990; Fink & Hicks 1996) was to systematically survey as many cometary emission lines as possible, so a lower spectroscopic resolving power was used than could effectively separate these emissions. The early work of Fink & Johnson (1984) used the van Dishoeck & Dalgarno (1984) value of BR3 to establish the dominance of H_2O in producing $\text{O}(^1D)$ over the central $\sim 5 \times 10^4$ km of the coma, to which their observing technique is typically sensitive. A standard model and reduction technique was adopted that relied on a Haser H_2O scale length of 8×10^4 km, which corresponds to the standard 8×10^4 s H_2O lifetime and a 1 km s^{-1} outflow velocity. Because extracting profiles from the [O I] measurements was difficult, Fink and coworkers adopted an innovative observational technique where the slit width was varied and aperture sums along the slit were considered (e.g., Hicks & Fink 1997). The left panel of Figure 6 shows Haser radial profiles generated with the parameters used by Fink and collaborators compared to a model generated using the parameters outlined above. These profiles, labeled "Fink," are scaled by the values listed in the legend. The right panel shows these profiles converted into aperture

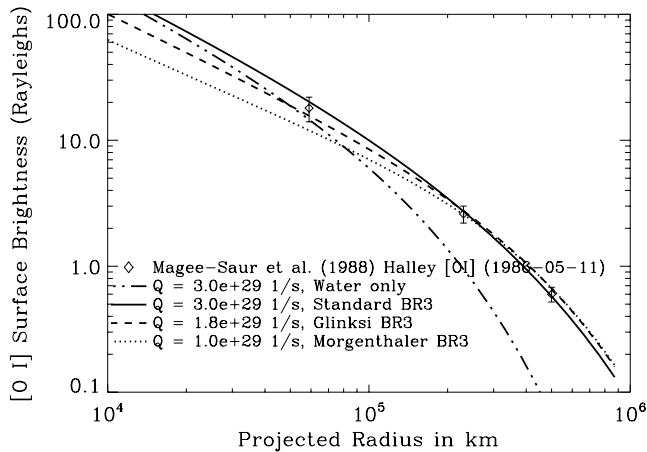


FIG. 7.—Wide-field comet Halley [O I] observations recorded on 1986 May 11 (Magee-Sauer et al. 1988) compared with various Haser models. The Haser model scale lengths were adjusted to emulate vectorial model profiles prepared with more physical parameters (see text). The $Q(\text{H}_2\text{O})$ values and photochemical assumptions for the models are shown in the legend. The H_2O and OH outflow velocities were derived using the method described in the text and were $v_{\text{H}_2\text{O}} = 0.64 \text{ km s}^{-1}$ and $v_{\text{OH}} = 1.2 \text{ km s}^{-1}$, respectively, for this date.

sums. Although the radial profiles are distinctly different in slope, the aperture sums are nearly identical for the case in which the assumed Fink model is scaled by a factor of 1.15. Any of the changes in the OH photochemistry proposed in Table 2 result in a noticeable flattening of our [O I] profile at large cometocentric distances, a shift in the peak of the aperture sum curve to larger cometocentric radii, and a noticeable tail on the aperture sum curve. The persistent use of their simple H_2O -only model suggests the data of Fink and collaborators does not support modification to the van Dishoeck & Dalgarno (1984) OH photochemistry.

4.2. Previous Fabry-Pérot Observations

Starting with comet C/1973 E1 (Kohoutek), there has been a long history of FP observations of cometary [O I] at the University of Wisconsin. Before the commissioning of the WHAM telescope, the most sensitive wide-field cometary [O I] measurements were conducted on 1986 May 11 when Halley was at a heliocentric distance of 1.78 AU (Magee-Sauer et al. 1988). We reproduce the Magee-Sauer et al. results in Figure 7 and compare them to Haser models generated with various photochemical assumptions. All of the models use H_2O and OH outflow velocities derived with the vectorial-to-Haser formulas of Combi et al. (2004) and equation (3). First, the dot-dot-dashed line shows that H_2O is unlikely to be the only source of [O I]. The solid line shows that the standard OH cross sections of van Dishoeck & Dalgarno (1984) converted to solar photochemical rates by Huebner et al. (1992) describes the measured points well, assuming an average $Q(\text{H}_2\text{O}) = 3 \times 10^{29} \text{ s}^{-1}$ for this FOV. The points are not inconsistent with the dashed line, which is produced using the OH photochemical rates of Glinski et al. (2004) and a lower $Q(\text{H}_2\text{O})$ value. The photochemical rates of Morgenthaler et al. (2001) result in the dotted line, which matches the outer points well, but begins to fall short of the inner point. The $Q(\text{H}_2\text{O})$ value of $1 \times 10^{29} \text{ s}^{-1}$ used in the Morgenthaler et al. case is close to the value of $9 \times 10^{28} \text{ s}^{-1}$ of Schleicher et al. (1998) for this day, assuming the efficiency of H_2O at producing OH to be 85.5% (BR2 in Table 1). As shown in Figure 2 of Schleicher et al. (1998), there is considerable variation in $Q(\text{H}_2\text{O})$ values determined by different methods. Particularly postperihelion, the Schleicher et al. $Q(\text{H}_2\text{O})$ values are, on average, a factor of 2–3 below those of

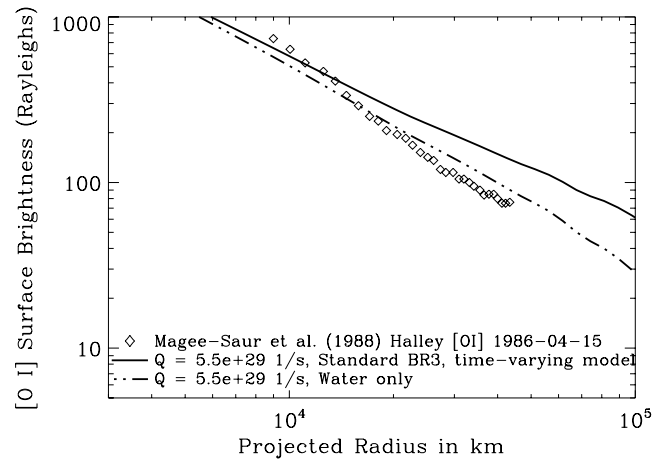


FIG. 8.—Comet Halley [O I] radial profile recorded on 1986 April 15 (Magee-Sauer et al. 1988) compared with the time-varying Haser model discussed in the text.

other methods. Feldman et al. (2004) show that the other methods for determining $Q(\text{H}_2\text{O})$ based on OH observations converge to the higher values. This, together with the observation by Magee-Sauer et al. (1988) that the innermost data point of Figure 7 is likely to be a lower limit, suggests that the Halley wide-field data does not support the modification to the OH photochemistry proposed by Morgenthaler et al. (2001).

In addition to [O I] observations in spectroscopic mode with a relatively small FOV ($2.5'$) offset various distances from the nucleus (Fig. 7), Magee-Sauer et al. (1988) recorded head-centered narrowband images of Halley with a $10'$ FOV. We reproduce the radial profiles of these images in Figures 8–10 (diamonds). The April 15 observation (Fig. 8) was taken nearly at the same time as long-slit observations were conducted by Fink and collaborators (e.g., Fink & Johnson 1984; Fink & Di Santi 1990; Fink & Hicks 1996). These observations are shown as the open circles in the right panel of Figure 1b of Combi & Fink (1993). Correcting for the fact that the y-axes are not calibrated to the same scale, we find a generally consistent slope between the two data sets. Magee-Sauer et al. fitted Haser profiles to the profiles in Figures 8–10 for two cases: (1) assuming H_2O was the only source of [O I] and (2) assuming H_2O and OH were both sources of [O I]. In both cases, the best-fit H_2O lifetimes were approximately a factor of 2 smaller than the solar-quiet value of Huebner et al. (1992). Magee-Sauer

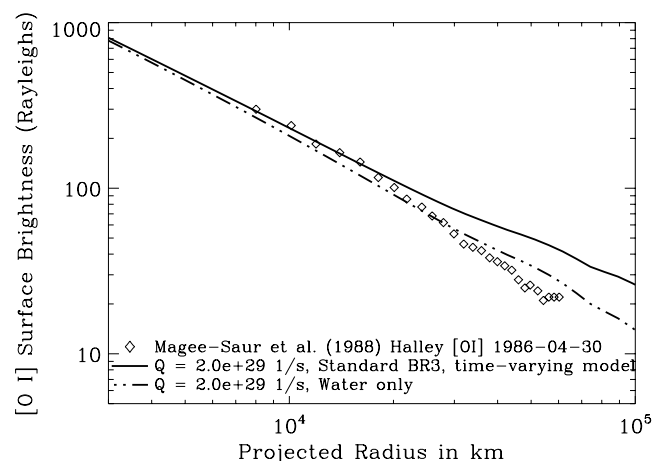


FIG. 9.—Same as Fig. 8, but recorded on 1986 April 30 (Magee-Sauer et al. 1988).

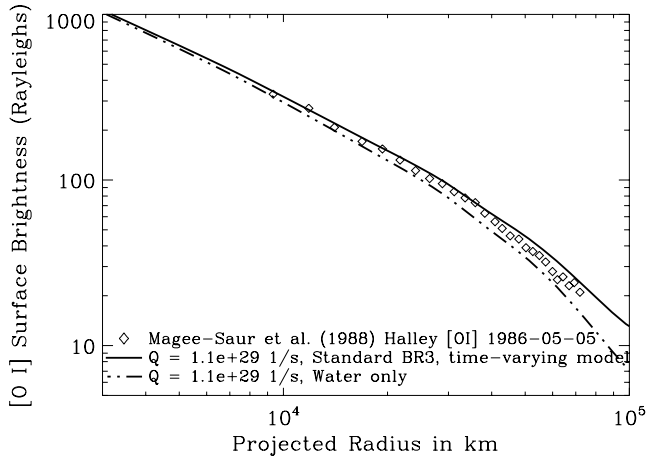


FIG. 10.— Same as Fig. 8, but recorded on 1986 May 5 (Magee-Saur et al. 1988).

et al. found longer lifetimes (although still short compared to those of Huebner et al.) when they used a time-varying Haser model, similar to that described above, to fit the profiles.

The time variation in $Q(\text{H}_2\text{O})$ used by Magee-Saur et al. (1988) to fit the profiles in Figures 8–10 was taken to be equivalent to the time variation in $Q(\text{C}_2)$, determined by Millis & Schleicher (1986). Schleicher et al. (1990) used a larger data set than Millis & Schleicher to determine the time-variability of $Q(\text{C}_2)$ to high accuracy in their $45''$ – $155''$ apertures. The phase and amplitude of this variation were projected back to the nucleus by Combi & Fink (1993) using low-resolution long-slit spectra with profiles extending out to 30,000 km in CN, C_2 , NH_2 , and $[\text{O I}]$. Combi & Fink found that in mid-April, their data were best fit by a phase advance of 6 hr and an amplitude increase of 27% of the Schleicher et al. $Q(\text{C}_2)$ periodogram. A larger CN data set confirmed these results, at least for that species (Combi et al. 1994).

To see if the proposed adjustment in the $Q(\text{C}_2)$ light curve phase and amplitude affects models of the $[\text{O I}]$ distribution measured by Magee-Saur et al. (1988), we use the adjusted $Q(\text{C}_2)$ periodogram and the time-varying Haser model described above to generate the model curves in Figures 8–10. The instantaneous production rate at the nucleus at the time of observation was adjusted so that the agreement between the model and the data was best at small radii, where the data presented by Combi et al. 1994 were collected. With the possible exception of the May 5 data, it is clear that model profiles produced in this way are too flat when compared to the data. In all cases, the modifications to the OH photochemistry suggested by Morgenthaler et al. (2001) and Glinski et al. (2004) produce model profiles that are clearly not consistent with the data. Assuming standard OH photochemistry, experimentation with the input parameters of the model shows that a longer phase advance, ~ 2 days and 1.25 days for April 15 and April 20, respectively, and no phase shift for May 5 provide better fits to the data. Consideration of the relationship between $Q(\text{C}_2)$ and $Q(\text{H}_2\text{O})$ in Halley is beyond the scope of this work, so we attach no physical significance to the phase shifts that result in better fits.

Using a similar FP system to that of Magee-Saur et al. (1988), Schultz et al. (1993) measured the $[\text{O I}]$ distribution in comet 1989 c1 (Austin). Unlike Halley, Hyakutake, and Hale-Bopp, the comet Austin apparition was during a time when the Sun was active. Schultz et al. use outflow velocity values, which are similar to ours, of $v_{\text{H}_2\text{O}} = 0.9 \text{ km s}^{-1}$ and $v_{\text{OH}} = 1.3 \text{ km s}^{-1}$. Using the lifetime of OH at 1 AU as a free parameter, Schultz et al. fit their $[\text{O I}]$ profiles. The typical fitted OH lifetime is $1.1 \pm 0.5 \times 10^5 \text{ s}$, which

is consistent with active Sun value of $1.1 \times 10^5 \text{ s}$ derived by Huebner et al. (1992). A substantial change in the OH photochemistry would significantly effect these results.

It is important to note that the total OH lifetime is a function not only of solar activity, but also of heliocentric velocity (the Swings effect). Using the experimentally determined OH cross sections of Brzozowski et al. (1978), Jackson (1980) was the first to consider this effect quantitatively, concentrating on predissociation of OH out of the $A^2\Sigma^+$ state, which is the dominant photo-destruction mechanism. Jackson found that the OH lifetime could vary by a factor of 3 over the heliocentric velocity range -58 to $+59 \text{ km s}^{-1}$. For several comets, the OH lifetimes calculated by Jackson were somewhat shorter than those inferred by cometary coma measurements. Perhaps because experimental difficulties similar to those of Brzozowski et al. (1978) the OH cross sections of Nee & Lee (1984) also result in an extremely short OH lifetime against solar photodissociation. The theoretically determined van Dishoeck & Dalgarno (1984) OH cross sections result in a longer OH lifetime, much more in agreement with cometary coma measurements (e.g., Nee & Lee 1984). Using van Dishoeck & Dalgarno cross sections, Schleicher & A'Hearn (1988, their Fig. 7) show that the total OH lifetime varies by no more than 25% due to the Swings effect for the comets we consider here. We have not found this variation to be sufficient to offset the effect of modifications to the standard OH photochemistry.

5. CONCLUSION

Spectroscopic observations of comet Hale-Bopp in $[\text{O I}]$ recorded with the WHAM telescope found a factor of 3–4 times more $[\text{O I}]$ than expected when compared to $[\text{O I}]$ production rates derived from $Q(\text{H}_2\text{O})$ values of other groups (e.g., Dello Russo et al. 2000; Colom et al. 1999; Combi et al. 2000) and standard H_2O and OH photochemistry (Morgenthaler et al. 2001). The WHAM observations, which were recorded over a sufficiently large FOV and with high enough sensitivity to eliminate the necessity for coma model-dependent aperture corrections, were verified by narrower field FP observations conducted at the McMath-Pierce solar telescope facility and multiobject spectrograph observations conducted at the WIYN telescope. In all, observations from four instruments at three telescopes support the report of $[\text{O I}]$ excess in Hale-Bopp, assuming standard OH photochemistry and instruments, such as *SOHO* SWAN (Combi et al. 2000), produced accurate $Q(\text{H}_2\text{O})$ values. In this work, we compare $[\text{O I}]$ measurements of comet Hyakutake recorded with WHAM to $[\text{O I}]$ production rates derived from *SOHO* SWAN $Q(\text{H}_2\text{O})$ values (Combi et al. 2005) and find that there is no evidence for an $[\text{O I}]$ excess (Table 3). The detailed shape of the $[\text{O I}]$ profile in Hyakutake is reasonably well fit by standard photochemistry and Haser outflow velocities (Figs. 3 and 5, *thick solid lines*). These profiles are not as well fit by any of the modifications to the OH photochemistry proposed to account for the excess $[\text{O I}]$ emission in Hale-Bopp (Morgenthaler et al. 2001; Glinski et al. 2004) unless the Haser outflow velocities are substantially less than accepted values. Similarly, $[\text{O I}]$ profiles from comet Austin (Schultz et al. 1993) are not well described by models constructed with modified OH photochemistry. Comet Halley presents a more enigmatic case. The three points in the wide-field $[\text{O I}]$ profile of Magee-Saur et al. (1988) are consistent with standard and modified OH photochemistry, with the resulting $Q(\text{H}_2\text{O})$ values consistent with the range of $Q(\text{H}_2\text{O})$ values found in the literature; however, as discussed in § 4.2, the lower $Q(\text{H}_2\text{O})$ values, and therefore the OH photochemistry of Morgenthaler et al. (2001), are not preferred. Because they have yet to be well fit by any model, it is difficult to make definitive statements about the Halley image-mode

[O I] data of Magee-Sauer et al. We simply observe that models with modified OH photochemistry result in poorer fits to the data. The bulk of the evidence suggests that the OH cross sections of van Dishoeck & Dalgarno (1984) are valid and Hale-Bopp was an exceptional comet. We assert that the treatment of gas phase chemical reactions by Glinski et al. (2004) was a step in the right direction toward understanding the excess [O I] emission in Hale-Bopp. Because the exothermal energy from some of the reactions listed in Table 1 of Glinski et al. (2004) may have important implications for coma dynamics, models of the Ly α coma may need to be revised, possibly modifying the *SOHO* SWAN-derived $Q(\text{H}_2\text{O})$ values. Other effects caused by Hale-Bopp's unusually high production rate would also be interesting to study with detailed models, such as the potential role Ly α opacity in the inner coma might have on position-dependent H $_2$ O and OH photodissociation rates.

Haser models, with parameters adjusted appropriately to emulate more sophisticated models (Combi et al. 2004) appear to adequately describe cometary [O I] radial profiles in the case in which there is no significant short-term time variation in production rates (e.g., Fink & Johnson 1984; Schultz et al. 1993; Fink & Hicks 1996). We show here that a time-varying Haser model, with $Q(\text{H}_2\text{O})$ values taken from the Ly α measurements of Combi et al. (2005) describes Hyakutake [O I] radial profile for measurements sensitive to both the inner (Fig. 3) and outer (Fig. 5) coma emissions. The same model, including the same photochemical assumptions, was not able to describe intermediate-field Halley [O I] observations (Figs. 8–10) when $Q(\text{H}_2\text{O})$ was taken to follow $Q(\text{C}_2)$ and reasonable photochemical rates were used. We suggest, therefore, that $Q(\text{C}_2)$ is not a high-precision proxy for $Q(\text{H}_2\text{O})$, at least in the case of Halley. This is in contrast to the claims of Combi & Fink (1993) and Smyth et al. (1995); however, the scatter in the [O I] profiles of Combi & Fink (their Figs. 1*b* and 2*b*) is very large and we find the $Q(\text{C}_2)$ and $Q(\text{H}_2\text{O})$ values plotted versus time in Figure 9 of Smyth et al. show similarity only in general trend. We must also consider the possibility that the Halley image-mode data of Magee-Sauer et al. is subject to systematic effects that vary with radial distance from the nucleus. However, the large separation in velocity space (relative to the instrument spectroscopic resolving power) of the airglow and cometary [O I] features for all the observations and robust flat-fielding tech-

niques (Oliversen 1983; Magee-Sauer 1988) confirms the confidence that Magee-Sauer et al. expressed in the data. Reconciliation of the high-precision Halley C $_2$ light curve of Schleicher et al. (1990) and the high-quality [O I] profiles of Magee-Sauer et al. (1988) will require a better understanding of the parentage of C $_2$ and possibly shed light on the relationship between H $_2$ O ice sublimation and the release of other volatiles from cometary nuclei.

In closing, we return to the arguments in § 1, which outlined the simplicity of using [O I] measurements to determine $Q(\text{H}_2\text{O})$ values in the cases in which [O I] production is dominated by H $_2$ O and OH photochemistry (e.g., not Hale-Bopp). In this work we have demonstrated that standard H $_2$ O and OH photochemistry, together with accepted H $_2$ O and OH Haser outflow velocities, produces radial profiles consistent with [O I] measurements for comets where $Q(\text{H}_2\text{O})$ is well understood. By using Fabry-Pérot spectrometers, or the newer Spatial Heterodyne Spectrometer (SHS) technique (e.g., Roesler & Harlander 1990; Mierkiewicz et al. 2004), sensitive high spectroscopic resolving power observations of comets over large FOVs are possible. With a large FOV, the need for aperture correction is diminished (i.e., AC \rightarrow 1), so direct conversion to $Q(\text{H}_2\text{O})$ using equations (1) and (2) is possible. Aperture mapping or imaging of the [O I] emission can be used to confirm model profiles used to derive AC in cases in which emission extends beyond the edge of the spectroscopic FOV. Imaging can also help identify unusual features, such as the yet-to-be-understood sunward extension in the [O I] distribution in comet Hale-Bopp (Morgenthaler et al. 2001, their Fig. 3). Finally, daily monitoring of comets in [O I] with FP or SHS instruments would yield time-accurate $Q(\text{H}_2\text{O})$ values, as variation in the nuclear production rate could be deconvolved from the time variation in the aperture photometry.

We would like to thank S. Tufte, L. M. Haffner for acquiring the Hyakutake data, M. Krok, K. Ripp for their efforts in data reduction, and D. Pierce for providing data tables of the radial profiles in Magee-Sauer et al. (1988). This work has been supported under NSF grant AST 09-615625, NASA grants NAG 05-7952, NNG 04-GN07G and NASA contract NASW-97020.

REFERENCES

- Brittacher, M., et al. 2001, *Geophys. Res. Lett.*, 28, 2561
 Brzozowski, J., Erman, P., & Lyyra, M. 1978, *Phys. Scr.*, 17, 507
 Budzien, S. A., Festou, M. C., & Feldman, P. D. 1994, *Icarus*, 107, 164
 Capria, M. T., Cremonese, G., Bhardwaj, A., & de Sanctis, M. C. 2005, *A&A*, 442, 1121
 Cochran, A. L., & Cochran, W. D. 2001, *Icarus*, 154, 381
 Colom, P., Gérard, E., Crovisier, J., & Bockelée-Morvan, D., Biver, N., & Rauer, H. 1999, *Earth Moon Planets*, 78, 37
 Combi, M. R., & Fink, U. 1993, *ApJ*, 409, 790
 Combi, M. R., Harris, W. M., & Smyth, W. H. 2004, in *Comets II*, ed. M. C. Festou, H. U. Keller, & H. A. Weaver (Tucson: Univ. of Arizona Press), 523
 Combi, M. R., Huang, B., Cochran, A., Fink, U., & Schulz, R. 1994, *ApJ*, 435, 870
 Combi, M. R., Mäkinen, J. T. T., Bertaux, J.-L., & Quemerais, E. 2005, *Icarus*, 177, 228
 Combi, M. R., Reinard, A. A., Bertaux, J., Quemerais, E., & Mäkinen, T. 2000, *Icarus*, 144, 191
 Crovisier, J. 1989, *A&A*, 213, 459
 Crovisier, J., Colom, P., Gérard, E., Bockelée-Morvan, D., & Bourgois, G. 2002, *A&A*, 393, 1053
 Dello Russo, N., Di Santi, M. A., Magee-Sauer, K., Gibb, E. L., Mumma, M. J., Barber, R. J., & Tennyson, J. 2004, *Icarus*, 168, 186
 Dello Russo, N., Di Santi, M. J., Magee-Sauer, K., Novak, R., & Rettig, T. W. 2000, *Icarus*, 143, 324
 Feldman, P. D., Cochran, A. L., & Combi, M. R. 2004, in *Comets II*, ed. M. C. Festou, H. U. Keller, & H. A. Weaver (Tucson: Univ. of Arizona), 425
 Festou, M. C. 1981, *A&A*, 95, 69
 Festou, M., & Feldman, P. D. 1981, *A&A*, 103, 154
 Fink, U., & Di Santi, M. A. 1990, *ApJ*, 364, 687
 Fink, U., & Hicks, M. D. 1996, *ApJ*, 459, 729
 Fink, U., & Johnson, J. R. 1984, *AJ*, 89, 1565
 Froese Fischer, C., & Saha, H. P. 1983, *Phys. Rev. A*, 28, 3169
 Glinski, R. J., Ford, B. J., Harris, W. M., Anderson, C. M., & Morgenthaler, J. P. 2004, *ApJ*, 608, 601
 Haffner, L. M., Reynolds, R. J., Tufte, S. L., Madsen, G. J., Jaehnig, K. P., & Percival, J. W. 2003, *ApJS*, 149, 405
 Harris, W. M., Scherb, F., Mierkiewicz, E. J., Oliversen, R. J., & Morgenthaler, J. P. 2002, *ApJ*, 578, 996
 Hicks, M. D., & Fink, U. 1997, *Icarus*, 127, 307
 Huebner, W. F., Keady, J. J., & Lyon, S. P. 1992, *Ap&SS* 195, 1
 Huppler, D., Reynolds, R. J., Roesler, F. L., Scherb, F., & Trauger, J. 1975, *ApJ*, 202, 276
 Jackson, W. M. 1980, *Icarus*, 41, 147
 Magee-Sauer, K. P. 1988, Ph.D. thesis, Univ. Wisconsin, Madison
 Magee-Sauer, K., Roesler, F. L., Scherb, F., Harlander, J., & Oliversen, R. J. 1988, *Icarus*, 76, 89
 Magee-Sauer, K., Scherb, F., Roesler, F. K., & Harlander, J. 1990, *Icarus*, 84, 154

- McPhate, J. B., Feldman, P. D., McCandliss, S. R., & Burgh, E. B. 1999, *ApJ*, 521, 920
- Mierkiewicz, E. J., Roesler, F. L., Harlander, J. M., Reynolds, R. J., & Jaehnig, K. P. 2004, *Proc. SPIE*, 5492, 751
- Millis, R. L., & Schleicher, D. G. 1986, *Nature*, 324, 646
- Morgenthaler, J. P., et al. 2001, *ApJ*, 563, 451
- Nee, J. B., & Lee, L. C. 1984, *J. Chem. Phys.*, 81, 31
- Oliversen, R. J. 1983, Ph.D. thesis, Univ. Wisconsin, Madison
- Reynolds, R. J. 1997, *Science*, 277, 1446
- . 2002, *Sci. Am.*, 286, 32
- Reynolds, R. J., Hausen, N. R., Tufte, S. L., & Haffner, L. M. 1998, *ApJ*, 494, L99
- Roesler, F. L., & Harlander, J. M. 1990, *Proc. SPIE*, 1318, 234
- Scherb, F. 1981, *ApJ*, 243, 644
- Schleicher, D. G., & A'Hearn, M. F. 1988, *ApJ*, 331, 1058
- Schleicher, D. G., Millis, R. L., & Birch, P. V. 1998, *Icarus*, 132, 397
- Schleicher, D. G., Millis, R. L., Thompson, D. T., Birch, P. V., Martin, R., Tholen, D. J., Piscitelli, J. R., Lark, N. L., & Hammel, H. B. 1990, *AJ*, 100, 896
- Schleicher, D. G., & Osip, D. J. 2002, *Icarus*, 159, 210
- Schultz, D., Li, G. S. H., Scherb, F., & Roesler, F. L. 1992, *Icarus*, 96, 190
- . 1993, *Icarus*, 101, 95
- Smyth, W. H., Combi, M. R., Roesler, F. L., & Scherb, F. 1995, *ApJ*, 440, 349
- Smyth, W. H., Marconi, M. L., Scherb, F., & Roesler, F. 1993, *ApJ*, 413, 756
- Streit, G. E., Howard, C. J., Schmeltekopf, A. L., Davidson, J. A., & Schiff, H. I. 1976, *J. Chem. Phys.*, 65, 4761
- van Dishoeck, E. F., & Dalgarno, A. 1984, *Icarus*, 59, 305
- Weaver, H. A., Feldman, P. D., Festou, M., A'Hearn, M. F., & Keller, H. U. 1981, *Icarus*, 47, 449